The dynamics of chimera states in heterogeneous Kuramoto networks

Carlo R. Laing [a]

[a] *Institute of Information and Mathematical Sciences, Massey University, Private Bag 102 904 NSMC, Auckland, New Zealand.*

Abstract

We study a variety of mixed synchronous/incoherent ("chimera") states in several heterogeneous networks of coupled phase oscillators. For each network, the recently-discovered Ott-Antonsen ansatz is used to reduce the number of variables in the PDE governing the evolution of the probability density function by one, resulting in a time-evolution PDE for a variable with as many spatial dimensions as the network. Bifurcation analysis is performed on the steady states of these PDEs. The results emphasise the commonality of the dynamics of the different networks, and provide stability information that was previously inferred.

Key words: Kuramoto, phase oscillators, synchrony, non-local, bifurcation.

1 Introduction

The dynamics of coupled oscillator networks has been of great interest for many years, with numerous applications from the biological and physical world [1–3]. One of the simplest such networks is the Kuramoto model, where each oscillator is described by a single angular variable (or phase), and the oscillators interact via a trigonometric function of phase differences [4–6]. Recently a number of authors have studied states in networks of identical Kuramoto oscillators for which some oscillators are synchronised with one another, while the remainder are incoherent [7–15], referred to by Abrams et al. as "chimera states." So far, four network topologies have been considered:

(1) A ring or line of oscillators with nonlocal coupling [12,7,10,9,11,14].

Email address: c.r.laing@massey.ac.nz (Carlo R. Laing).

(2) A two-dimensional array of oscillators with nonlocal coupling [15].
(3) An all-to-all coupled network, but with inhomogeneous coupling strengths [13].
(4) Two subnetworks, with all-to-all coupling both within and between subnetworks [8,12].

The first analysis of such states was performed by Kuramoto and Battogtokh (KB) [14], who considered a ring of oscillators. These authors defined an order parameter in terms of the states of the oscillators, wrote the dynamics of the oscillators in terms of this order parameter, and solved for the order parameter in a self-consistent manner, thus showing that such states existed. Abrams et al. [7,10] then analysed the functional equation derived by KB [14], showed that it was equivalent, in a particular case, to four scalar equations and investigated how solutions of these equations changed as parameters were varied. They found that chimera states bifurcated from states with no spatial structure. More recently, Omel'chenko et al. [11] and Sethia et al. [9] performed a similar analysis to KB [14] but including delays.

Shima and Kuramoto [15] considered a two-dimensional array of phase oscillators and found spiral waves with "phase-randomised cores." Most of the oscillators (involved in the spiral) were synchronised, having the same frequency but different phases, while the remainder (at the spiral's core) were incoherent, with seemingly independent phases. These authors performed a similar analysis to KB [14], deriving an equation to be solved self-consistently and showing that solutions of this equation agreed with simulations of the full system.

Ko and Ermentrout [13] considered a network of all-to-all coupled oscillators, but with coupling strengths chosen from a power-law distribution. They found partially-locked states and analysed them using the self-consistency approach of KB [14].

In refs. [13,11,7,10,12] bifurcation diagrams are shown, with stability of solutions marked. However, these stabilities all seem to have been inferred rather than calculated. Stable states are found through simulation of the network of oscillators and the corresponding branch of solutions of the self-consistent equation is identified as stable. Turning points on curves of solutions are assumed to be saddle-node bifurcations, resulting in unstable branches of solutions. Abrams et al. [8] were the first to consider the dynamics of (i.e. stability of) chimera states, analysing a system comprised of two sub-networks. They used the recent discovery of Ott and Antonsen (OA) [16], that certain networks of phase oscillators have low-dimensional dynamics, to derive a pair of nonlinear ODEs exactly describing chimera states in their network. The stability of such solutions and their bifurcations were investigated. However, Pikovsky and Rosenblum [17] showed

using the approach of Watanabe and Strogatz [18] that the results in [8] were incomplete.

All of the papers [7–11,13–15] considered networks of identical oscillators. In contrast, Laing [12] considered chimera states in networks of nonidentical oscillators (with intrinsic frequencies chosen from a distribution) and found that — within limits — chimeras are robust to heterogeneity. Laing [12] also provided evidence to support the observation of Martens et al. [19] and Pikovsky and Rosenblum [17] that the OA ansatz [16] correctly predicts the dynamics of Kuramoto-type networks when the oscillators have randomly-distributed frequencies.

In this paper we use the OA ansatz to derive equations describing the dynamics of the networks referred to in points 1-3 above, when the networks are heterogeneous, and analyse these equations. This work greatly extends that in [12] and demonstrates that all of the networks in points 1-4 above can be analysed in the same way.

In Sec. 2 we consider the ring topology of Kuramoto and Battogtokh [14] and others, putting on a solid footing the stability results of Laing [12], showing that Hopf bifurcations can occur in such systems, and that Hopf and saddle-node bifurcations are arranged in parameter space around a Takens-Bogdanov point. In Sec. 3 we consider a network with power-law distributed coupling strengths, and recover results similar to those of Ko and Ermentrout [13]. In Sec. 4 we consider spiral waves in two spatial dimensions, deriving a number of new results. Two models similar to that studied in Sec. 2 are investigated in Sec. 5, and we reproduce some results of others, although using a different approach. We conclude in Sec. 6.

2 A ring of oscillators

Consider a ring of N phase oscillators with nonlocal coupling [12,7,10,14]. For this network a chimera state refers to a statistically-stationary state for which oscillators on part of the ring are synchronised while those on the rest of the ring are incoherent. See Fig. 1 for an example.

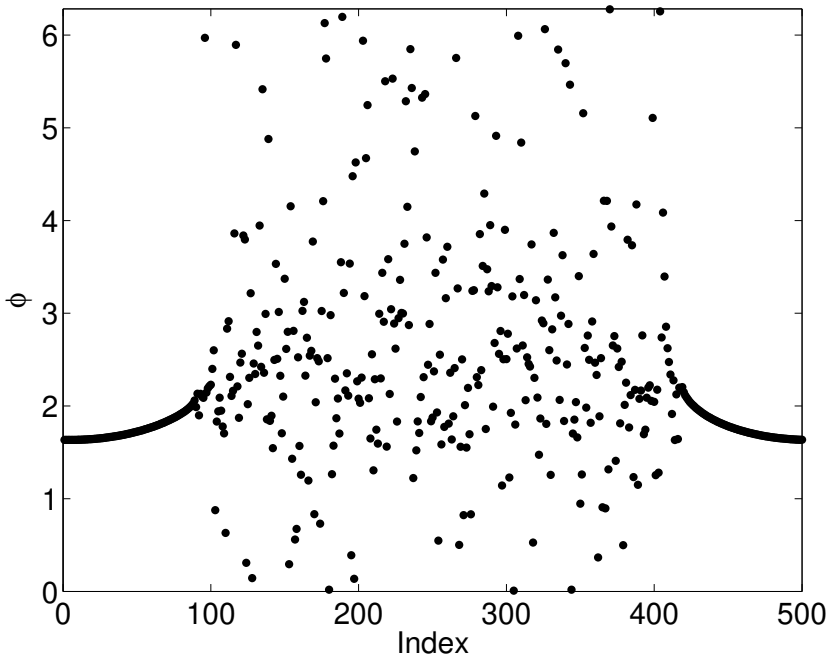

Fig. 1. A snapshot of a chimera solution of the system (1). $N = 500, \beta = 0.2$ and the ω_i are taken from a Dirac delta distribution. $G(x) = (1 + 0.95 \cos x)/(2\pi)$.

2.1 Analysis

The system is

$$\frac{d\phi_i}{dt} = \omega_i - \frac{2\pi}{N} \sum_{j=1}^{N} G\left(\frac{2\pi|i-j|}{N}\right) \cos\left(\phi_i - \phi_j - \beta\right) \tag{1}$$

for $i = 1, \ldots N$, where ϕ_i is an angular variable and the natural frequencies ω_i are chosen from a distribution $g(\omega)$. The coupling function G is periodic with period 2π.

We move to the continuum limit ($N \to \infty$) and assume there is a probability density function $f(x, \omega, \phi, t)$ characterising the state of the system. This function satisfies the continuity equation [8,6]

$$\frac{\partial f}{\partial t} + \frac{\partial}{\partial \phi}(fv) = 0 \tag{2}$$

where

$$v = \omega - \int_0^{2\pi} G(x-y) \int_{-\infty}^{\infty} \int_{-\pi}^{\pi} \cos\left[\phi - \phi' - \beta\right] f(y, \omega, \phi', t) d\phi' d\omega dy \tag{3}$$

and $\phi = \phi(x)$ and $\phi' = \phi(y)$. Defining the order parameter

$$R(x,t) \equiv \int_0^{2\pi} G(x-y) \int_{-\infty}^{\infty} \int_{-\pi}^{\pi} e^{-i\phi'} f(y,\omega,\phi',t) d\phi' \, d\omega \, dy \tag{4}$$

we can rewrite

$$v = \omega - \frac{1}{2}\left[R e^{i(\phi-\beta)} + \overline{R} e^{-i(\phi-\beta)} \right] \tag{5}$$

where an overbar indicates complex conjugate. Following Ott and Antonsen [16], we write

$$f(x,\omega,\phi,t) = \frac{g(\omega)}{2\pi}\left[1 + \left\{ \sum_{n=1}^{\infty} h_n(x,\omega,t) e^{in\phi} + c.c. \right\} \right] \tag{6}$$

where "$c.c.$" indicates the complex conjugate of the previous term, and assume that $h_n(x,\omega,t) = [a(x,\omega,t)]^n$, i.e. that the nth coefficient is a function, $[a(x,\omega,t)]$, raised to the nth power. Substituting (6) into (2) we obtain

$$\frac{\partial a}{\partial t} = -i\omega a + (i/2)\left[R e^{-i\beta} + \bar{R} e^{i\beta} a^2 \right] \tag{7}$$

where

$$R(x,t) = \int_{-\pi}^{\pi} G(x-y) \int_{-\infty}^{\infty} g(\omega) a(y,\omega,t) \, d\omega \, dy \tag{8}$$

This ansatz, which effectively replaces the infinite set of functions, $\{h_n\}$ by a single function, a, is non-trivial, and its validity is discussed in Sec. 6.

In this paper we will always assume that the ω are chosen from a Lorentzian distribution with half-width-at-half-maximum D, i.e.

$$g(\omega) = \frac{D/\pi}{(\omega-\omega_0)^2 + D^2} = \frac{1}{2\pi i}\left(\frac{1}{\omega - \omega_0 - iD} - \frac{1}{\omega - \omega_0 + iD} \right) \tag{9}$$

where ω_0 is the centre of the distribution. For non-delayed, autonomous systems we can always set $\omega_0 = 0$ without loss of generality, by moving to a rotating coordinate frame. With $g(\omega)$ from (9) and $\omega_0 = 0$ we can use contour integration to perform the integral over ω in (8), obtaining [12,16]

$$R(x,t) = \int_{-\pi}^{\pi} G(x-y) a(y, -iD, t) \, dy \tag{10}$$

Writing $\tilde{z}(x,t) = a(x,-iD,t)$ we have

$$\frac{\partial \tilde{z}}{\partial t} = -D\tilde{z} + (i/2)\left[R e^{-i\beta} + \bar{R} e^{i\beta} \tilde{z}^2 \right] \tag{11}$$

where

$$R(x,t) = \int_{-\pi}^{\pi} G(x-y) \tilde{z}(y,t) \, dy \tag{12}$$

As is known [7,12,14], the analysis of (11)-(12) is simplified by moving to a rotating coordinate frame (rotating in the ϕ direction, not x). Thus we define $z \equiv \tilde{z}e^{i\Omega t}$, where Ω is as yet unknown. We find that z satisfies

$$\frac{\partial z}{\partial t} = (i\Omega - D)z + (i/2)\left[\widehat{R}e^{-i\beta} + \overline{\widehat{R}}e^{i\beta}z^2\right] \tag{13}$$

where

$$\widehat{R}(x,t) = \int_{-\pi}^{\pi} G(x-y)z(y,t)\,dy \tag{14}$$

As other authors have done [7,10,12] we assume that $G(x) = (1+A\cos x)/(2\pi)$, and that z is even in x. Then, henceforth dropping the hat on $\widehat{R}$, we have

$$R(x,t) = z_0(t) + z_1(t)\cos x \tag{15}$$

where

$$z_0(t) = \frac{1}{2\pi}\int_0^{2\pi} z(x,t)\,dx \quad \text{and} \quad z_1(t) = \frac{A}{2\pi}\int_0^{2\pi} z(x,t)\cos(x)\,dx \tag{16}$$

We are interested in stationary solutions of (13)-(14), their stability and the bifurcations they undergo as parameters are varied. A stationary solution of (13) is a function $z(x)$ which satisfies

$$(i\Omega - D)z + (i/2)\left[Re^{-i\beta} + \overline{R}e^{i\beta}z^2\right] = 0 \tag{17}$$

where R is also independent of time. Note that for any solution z of (17), $ze^{i\psi}$, where ψ is arbitrary, is also a solution of (17). We can compare these stationary solutions with those already found using a self-consistency argument [12,7]. Solving (17) for z we obtain

$$z = \frac{D - i\Omega \pm \sqrt{(D-i\Omega)^2 + |R|^2}}{i\overline{R}e^{i\beta}} \tag{18}$$

Choosing the negative square root and taking the spatial average of (18) we obtain

$$z_0 = \frac{1}{2\pi}\int_0^{2\pi} \frac{D - i\Omega - \sqrt{(D-i\Omega)^2 + |R(x)|^2}}{i\overline{R}(x)e^{i\beta}}dx \tag{19}$$

which (up to the allowable arbitrary rotation of z in the complex plane [7]) is the same as equation (28) in [12]. Similarly, multiplying both sides of (18) by $A\cos x$ and integrating we obtain

$$z_1 = \frac{A}{2\pi}\int_0^{2\pi}\left(\frac{D - i\Omega - \sqrt{(D-i\Omega)^2 + |R(x)|^2}}{i\overline{R}(x)e^{i\beta}}\right)\cos(x)\,dx \tag{20}$$

which (after the same arbitrary rotation mentioned above) is the same as equation (29) in [12]. The self-consistency argument of others [12,7,10] consists of simultaneously solving (19)-(20) for the scalars z_0, z_1 and Ω. This

self-consistency argument shows that chimera states exist, but does not give any information about the dynamics and stability of such solutions.

Now consider the physical interpretation of solutions of (17). Considering stationary states in the coordinate frame rotating with angular velocity Ω and fixing $\omega = -iD$, we see that the probability density function $F(\phi)$ at position x has proportionality

$$F(\phi) \sim \sum_{n=-\infty}^{\infty} [z(x)]^n e^{in\phi} \tag{21}$$

Note that for this series to converge we must have $|z| \leq 1$. Now if $z = re^{-i\theta}$, where $0 \leq r < 1$, we have

$$F(\phi) = \frac{1 - r^2}{2\pi[1 - 2r\cos(\phi - \theta) + r^2]}, \tag{22}$$

the Poisson kernel, whereas if $r = 1$ we have

$$F(\phi) = \delta(\phi - \theta), \tag{23}$$

the Dirac delta function. Thus θ gives the value of ϕ at which the maximum of F occurs, and r is a measure of the "peakedness" of the distribution; $r = 0$ corresponds to a uniform distribution, while $r = 1$ corresponds to the Dirac delta. This physical interpretation also shows why solutions of (17) are invariant under the rigid rotation $z \mapsto ze^{i\psi}$ mentioned above — it is just a manifestation of the invariance of the full system (1) under the shift $\phi_i \mapsto \phi_i + \psi \ \ \forall i$.

2.2 Results

We now discuss numerical solutions of (13)-(14). To find them, the domain is discretised into 500 evenly-spaced points and the corresponding ODEs are then solved. A typical solution is shown in Fig. 2, where we write $z = re^{-i\theta}$. Note that $\theta(x)$ is only specified up to a shift, so we set $\theta(0) = 0$. Recall that values of r close to 1 (at both ends of the domain) correspond to tightly synchronised oscillators, while lower values of r (in the centre of the domain) correspond to less coherent oscillators. While the correspondence with the state in Fig. 1 is not exact, due to the non-zero value of D used here, the general features are the same.

Figure 3 shows another representation of the solution in Fig. 2. Here we

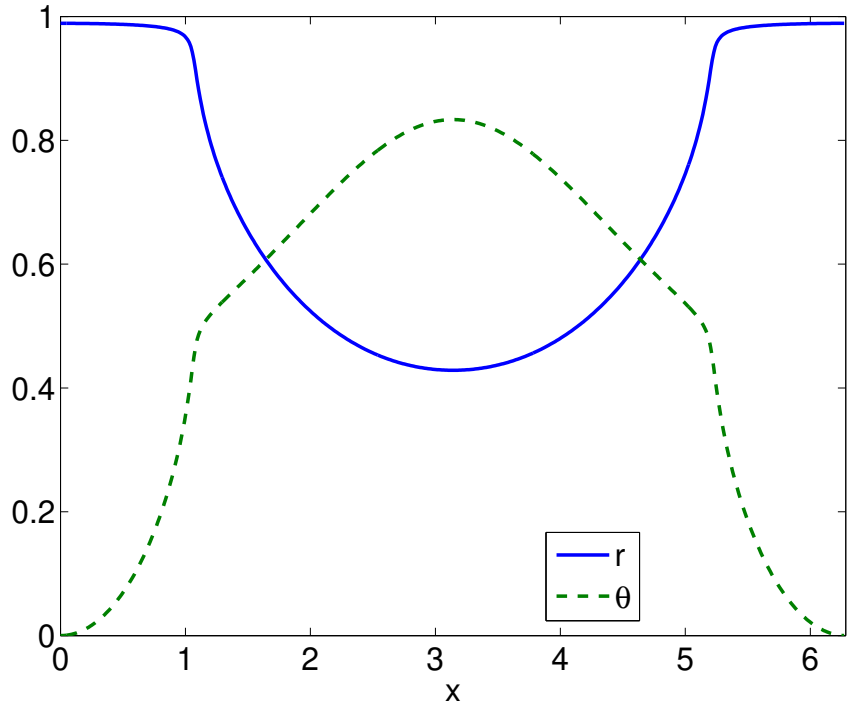

Fig. 2. A stable stationary solution of (13)-(14) with $\Omega = -0.74051$ ($z = re^{-i\theta}$). Other parameters: $A = 0.95, \beta = 0.2, D = 0.004$.

show $\log[\widetilde{F}(x,\phi)]$ using a colour code, where

$$\widetilde{F}(x,\phi) \equiv \frac{1-r^2(x)}{2\pi[1-2r(x)\cos(\phi-\theta(x))+r^2(x)]} \tag{24}$$

(cf. (22)) is the probability density function. Black corresponds to high probability, white to low. We again set $\theta(0) = 0$. Keeping in mind that $D \neq 0$ here, the correspondence between the state in Fig. 1 and the data in Fig. 3 is clear.

2.2.1 Continuation

Figure 4 shows the results of following solutions of (13)-(14) for fixed D and A. We plot the difference between the maximum over x of r and the minimum over x of r as a function of β. Stability, as given by the most positive real part of the eigenvalues of the linearisation of (13) about a solution, is indicated. Note that due to the invariance under a shift in θ there will always be an eigenvalue of zero. Figure 5 shows $r(x)$ and $\theta(x)$ at the four points on the curve indicated in Fig. 4.

Figure 4 also shows a branch of spatially uniform solutions, and their stability. For these solutions $R = z$ and from (17) we see that they satisfy the

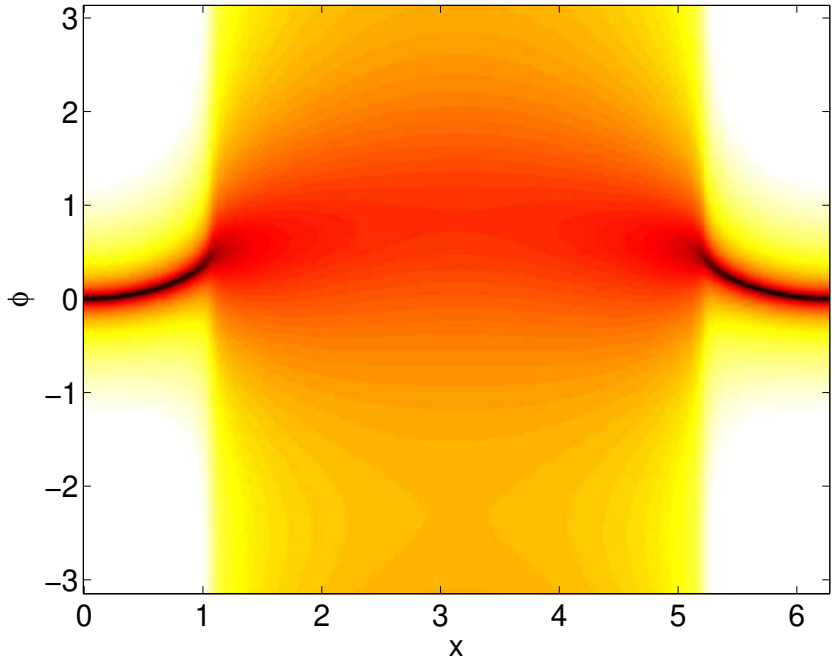

Fig. 3. Another representation of the solution shown in Fig. 2. Black corresponds to high probability, white to low. See text for more details.

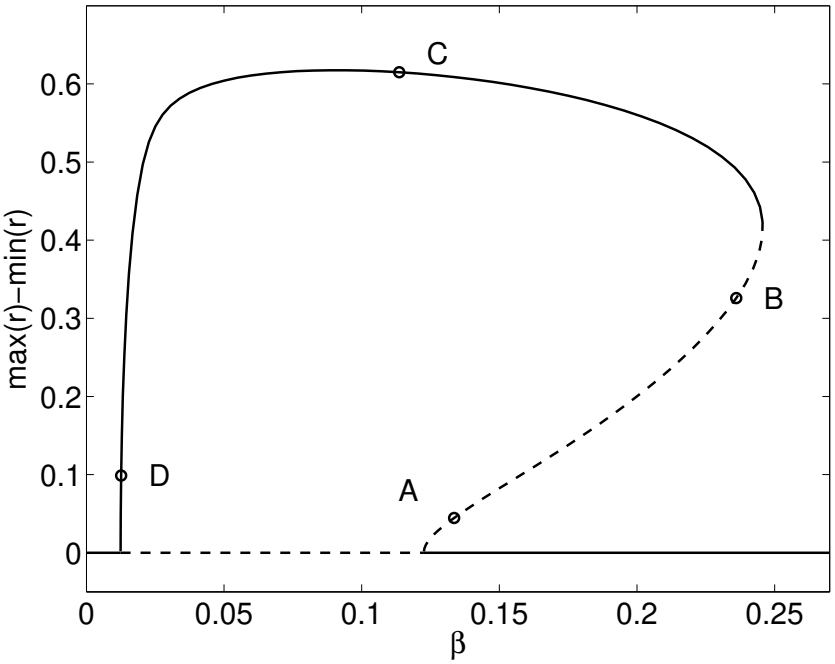

Fig. 4. $\max(r) - \min(r)$ as a function of β for stationary solutions of (13)-(14). Solid line: stable; dashed line: unstable. $r(x)$ and $\theta(x)$ at the four points indicated are plotted in Fig. 5. Parameters are $D = 0.004, A = 0.95$.

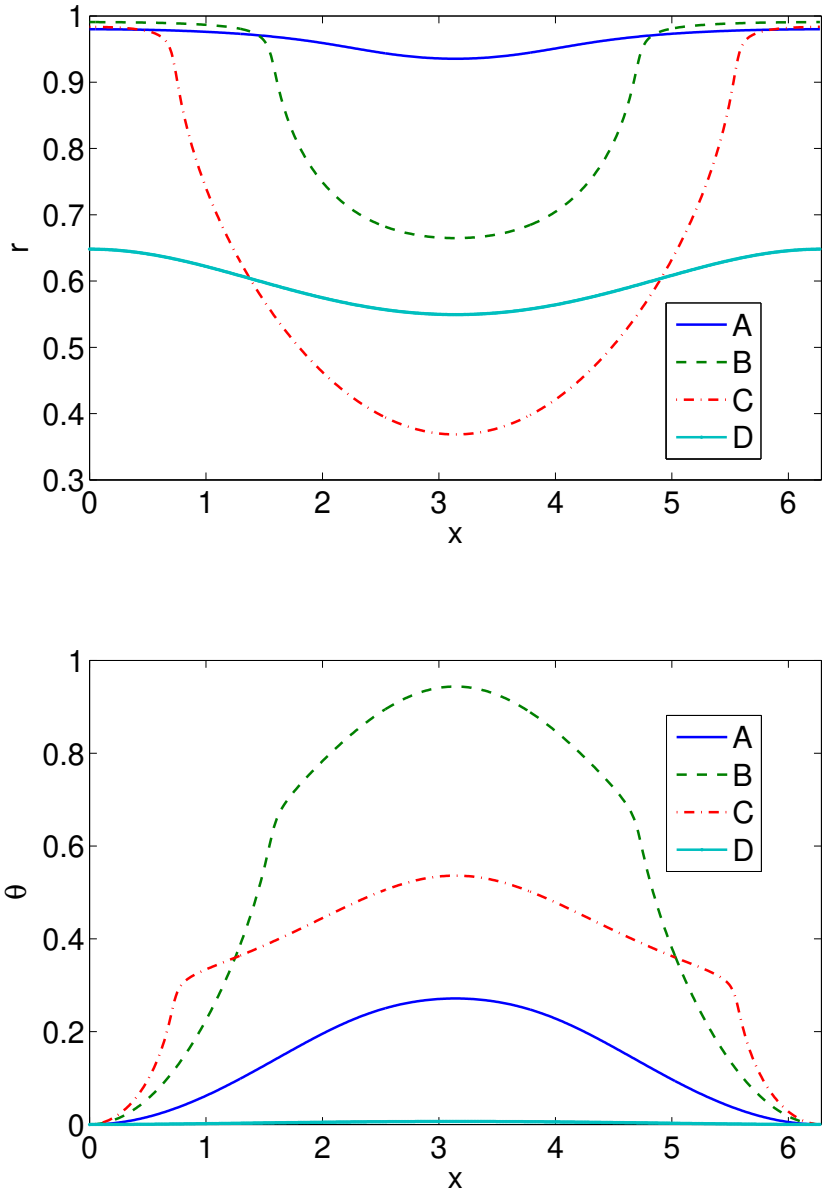

Fig. 5. Top: $r(x)$ and bottom: $\theta(x)$ at the four points indicated in Fig. 4. Note that we fix $\theta(0) = 0$.

complex scalar equation

$$i\Omega - D + (i/2)\left[e^{-i\beta} + r^2 e^{i\beta}\right] = 0 \tag{25}$$

The results in Fig. 4 agree with those in [12], but the new result here is that the stability of curves in Fig. 4 has been calculated using the eigenvalues of the linearisation of (13) about a solution, rather than inferred, as was the case in [12]. In principle we could follow the pitchfork and saddle-node bifurcations in Fig. 4 as another parameter (e.g. D) was varied, obtaining results such as those in [12], but we do not do that here.

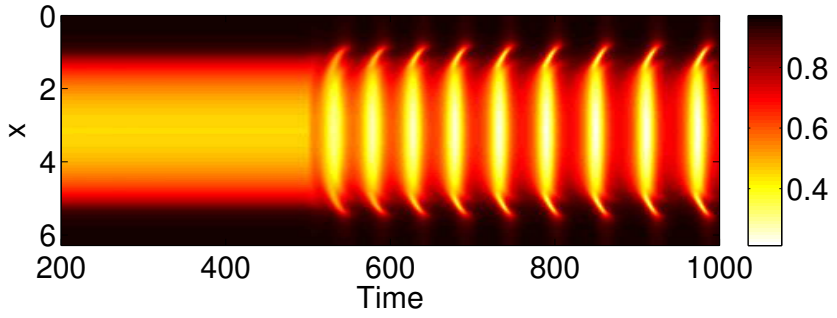

Fig. 6. A Hopf bifurcation in (13)-(14) caused by increasing β_1 from 0 to 0.1 at $t = 500$. The colour encodes r. Other parameters: $A = 0.95, D = 0.015, \beta_0 = 0.2$.

2.2.2 *Hopf bifurcations*

One of the questions posed in [8] was: do breathing (i.e. oscillating) chimeras exist in one-dimensional arrays of oscillators such as the one studied in this section? Here we answer this question in the affirmative by introducing parameter heterogeneity, letting $\beta(x) = \beta_0 - \beta_1 \cos(x)$ in (13)-(14). Figure 6 shows an apparent Hopf bifurcation as β_1 is abruptly increased from zero. To verify that this bifurcation also occurs in the network of oscillators, (1), we performed the same change in parameters and the results are shown in Fig. 7. The top panel shows $\sin(\phi_i)$ as a function of time and the bottom panel shows $|R_i|$ as a function of time, where R_i is the spatially-discrete version of $R(x,t)$, defined using (4) as

$$R_k(t) = \frac{2\pi}{N} \sum_{j=1}^{N} G\left(\frac{2\pi|k-j|}{N}\right) e^{-i\phi_j} \tag{26}$$

The onset of oscillations in the discrete network is clear.

Figure 8 shows the real part of the rightmost few eigenvalues of the linearisation of (13) about a solution similar to the initial condition shown in Fig. 6, as a function of β_1. The crossing of the imaginary axis by a pair of complex conjugate eigenvalues as β_1 increases through approximately 0.085 is clear. (The imaginary part of these eigenvalues, not shown, varies between approximately $0.13i$ and $0.15i$ over the parameter range shown.) The zero eigenvalue mentioned above is also evident.

In Fig. 9 we show the curves of Hopf bifurcations in the (β_0, β_1) plane. Also shown is the continuation of the saddle-node bifurcation that occurs when $\beta_1 = 0$ (see Fig. 4). These curves meet at a Takens-Bogdanov (double-zero eigenvalue) bifurcation. Generically, one expects a curve of homoclinic bifurcations to emanate from a Takens-Bogdanov point [20,21]. Figure 10 shows evidence that such a curve does exist in this case, lying above the curve of Hopf bifurcations, just as in Fig. 4 of [8]. In Fig. 10 we show $r(\pi)$ (i.e. in the middle of the domain) as a function of time for successively in-

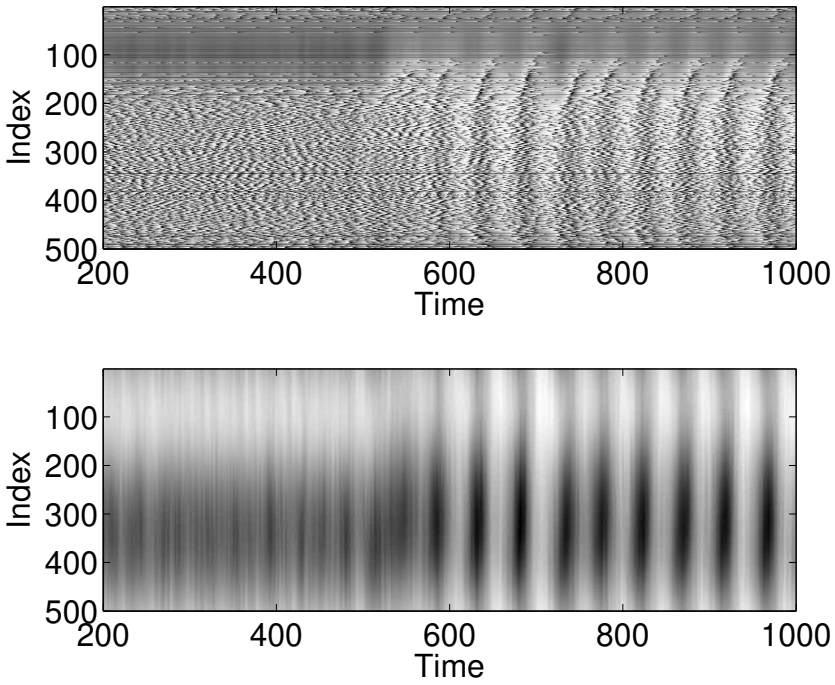

Fig. 7. A Hopf bifurcation in (1) caused by increasing β_1 from 0 to 0.1 at $t = 500$. Top: $\sin \phi_i$. Bottom: magnitude of the discrete order parameter, $|R_i|$, as defined in the text. Compare with Fig. 6. Other parameters: $A = 0.95, D = 0.015, \beta_0 = 0.2$.

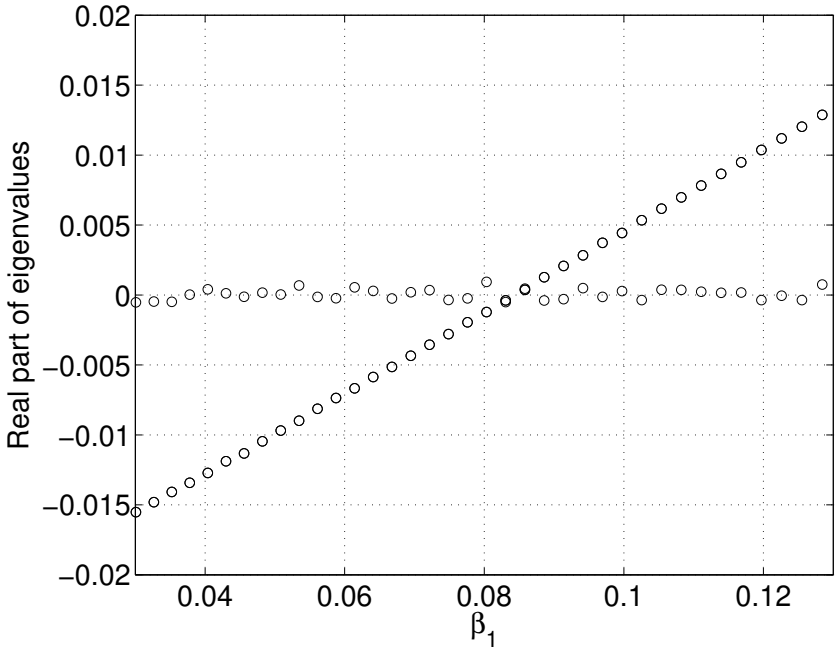

Fig. 8. Real part of the rightmost few eigenvalues of the linearisation of (13) about one of its solutions as a function of β_1. Other parameters: $A = 0.95, D = 0.015, \beta_0 = 0.2$.

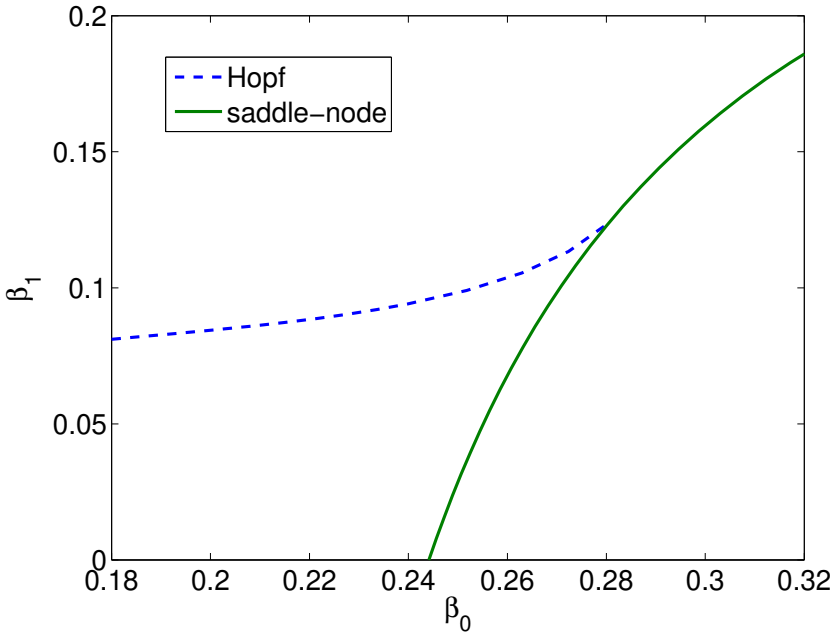

Fig. 9. Curves of Hopf (dashed) and saddle-node (solid) bifurcations of nontrivial solutions of (13)-(14). Nontrivial solutions exist to the left of the saddle-node curve and are stable below the Hopf curve. Other parameters: $A = 0.95, D = 0.015$.

creasing values of β_1, when $\beta_0 = 0.2$, i.e. moving up a vertical line in Fig. 9. The period of oscillation increases as β_1 increases and for even higher values of β_1 the system moves to a stationary, nearly spatially-uniform, state (not shown). Both of these are consistent with a homoclinic bifurcation. The homoclinic bifurcation could presumably be followed using the package HOMCONT [22].

Note that by assuming that z is even in x, we are selecting one out of a continuum of states, each related by a rotation around the ring, thus "pinning" the solution. If this condition was relaxed it may be possible to obtain bifurcations to drifting states, for which the pattern moves at a constant speed around the ring [23].

In summary, we have used the OA ansatz to re-establish a result of [12], namely that the steady states of (13)-(14) satisfy (19)-(20). New results include the derivation of the stabilities shown in Fig. 4, the investigation of Hopf bifurcations, and the two-parameter diagram shown in Fig. 9.

3 Inhomogeneous coupling

We now consider another type of network, with all-to-all coupling and heterogeneous coupling strengths. Ko and Ermentrout [13] recently studied

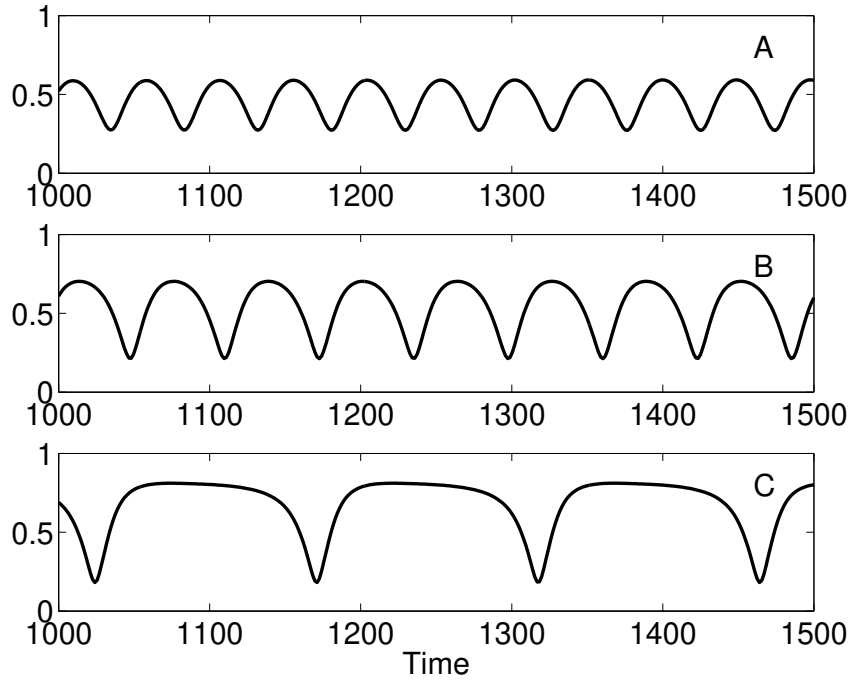

Fig. 10. A plot of $r(\pi)$ as a function of time for (A): $\beta_1 = 0.09$, (B): $\beta_1 = 0.1$, (C): $\beta_1 = 0.1125$. Other parameters: $A = 0.95, D = 0.015, \beta_0 = 0.2$.

the following model

$$\frac{\mathrm{d}\phi_i}{\mathrm{d}t} = \omega_i + \frac{K_i}{N}\sum_{j=1}^{N} H(\phi_j - \phi_i) \tag{27}$$

where $H(\phi) = \sin(\phi - \beta) + \sin\beta$ and the K_i are taken from a truncated power-law distribution $\Gamma(K)$, where

$$\Gamma(K) = \begin{cases} CK^{-\gamma} & \text{for } K \in [K_{min}, K_{max}] \\ 0 & \text{otherwise} \end{cases} \tag{28}$$

and C is a normalising factor such that $\int_0^\infty \Gamma(K)dK = 1$. As before, let the ω_i be chosen from the probability density function $g(\omega)$. These authors found that for certain ranges of parameters (and identical ω_i) partial locking, in which some fraction of the oscillators synchronise, occurs. An example of such partial locking is shown in Fig. 11, where we have ordered the oscillators by their K value. We see that it is oscillators with low K which synchronise, oscillators with higher K have higher average frequency, and that the synchronous oscillators do not rotate with the intrinsic frequency of the oscillators, ω_i, which are all zero in this case.

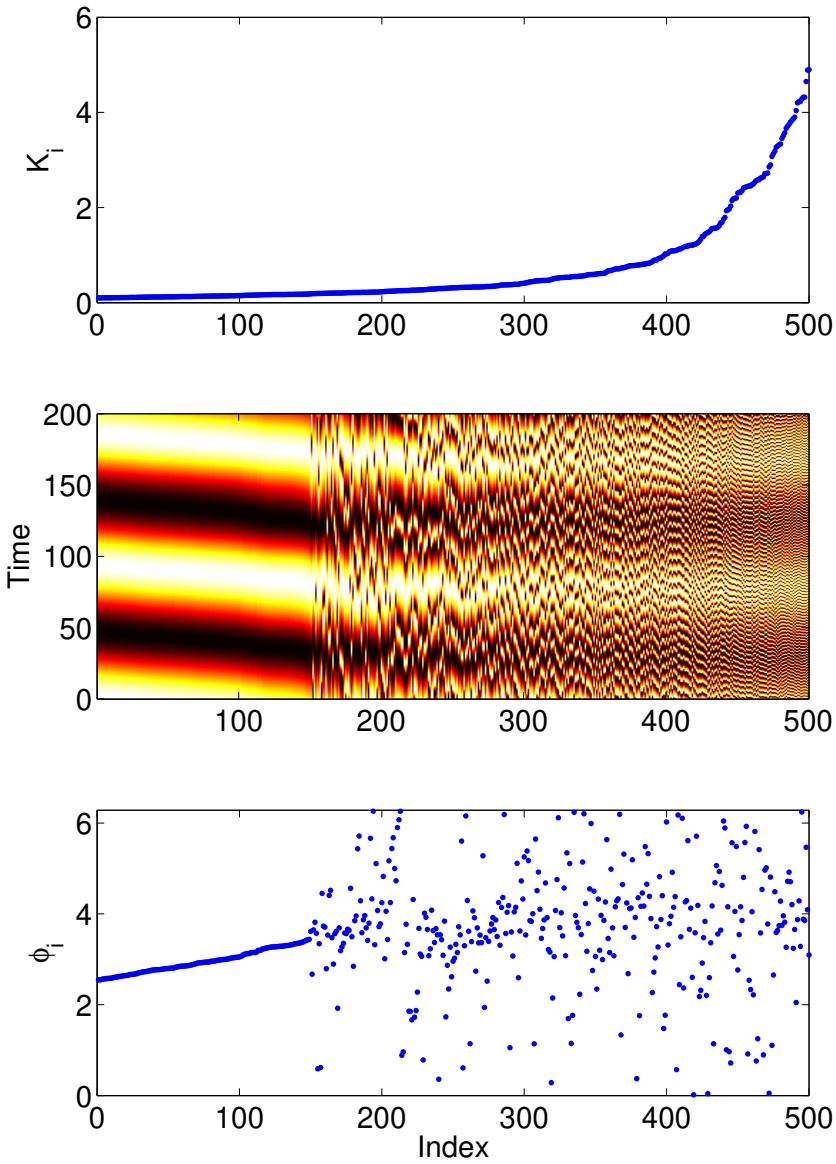

Fig. 11. Top: K_i versus oscillator index. Middle: $\sin\phi_i$ (colour–coded) over a time interval of length 200. Bottom: a snapshot of the phases ϕ_i. Transients have been removed. Other parameters: $N = 500, K_{min} = 0.1, K_{max} = 5, \gamma = 1.5, \beta = 0.4\pi, \omega_i = 0 \ \forall i$.

3.1 Analysis

We now analyse the continuum limit of (27). The analysis is analogous to that in Sec. 2.1, but the variable x is now replaced by K. First rewrite (27) as

$$\frac{\mathrm{d}\phi_i}{\mathrm{d}t} = \omega_i + K_i \sin\beta + \frac{K_i}{N}\sum_{j=1}^{N}\sin(\phi_j - \phi_i - \beta) \tag{29}$$

In the continuum limit, we again assume the existence of a probability density function $f(K, \omega, \phi, t)$ which satisfies the continuity equation

$$\frac{\partial f}{\partial t} + \frac{\partial}{\partial \phi}(fv) = 0 \tag{30}$$

where

$$v = \omega + K \sin\beta + K \int_0^\infty \Gamma(K) \int_{-\infty}^\infty \int_0^{2\pi} \sin\left[\phi' - \phi - \beta\right] f(K, \omega, \phi', t) d\phi' \, d\omega \, dK \tag{31}$$

Defining the (scalar) order parameter

$$R(t) = \int_0^\infty \Gamma(K) \int_{-\infty}^\infty \int_0^{2\pi} e^{i\phi'} f(K, \omega, \phi', t) d\phi' \, d\omega \, dK \tag{32}$$

we can write

$$v = \omega + K \sin\beta + \frac{K}{2i}\left[Re^{-i(\phi+\beta)} - \overline{R}e^{i(\phi+\beta)}\right] \tag{33}$$

As before, we use the OA ansatz to write

$$f(K, \omega, \phi, t) = \frac{g(\omega)}{2\pi}\left[1 + \left\{\sum_{n=1}^\infty [a(K, \omega, t)]^n e^{in\phi} + c.c.\right\}\right] \tag{34}$$

and substitute this into (30) and (32) to obtain

$$\frac{\partial a}{\partial t} = -i(\omega + K\sin\beta)a + (K/2)\left[\overline{R}e^{i\beta} - Re^{-i\beta}a^2\right] \tag{35}$$

where

$$R(t) = \int_0^\infty \Gamma(K) \int_{-\infty}^\infty g(\omega)\overline{a}(K, \omega, t) \, d\omega \, dK \tag{36}$$

If

$$g(\omega) = \frac{D/\pi}{\omega^2 + D^2} \tag{37}$$

then

$$R(t) = \int_0^\infty \Gamma(K)\overline{a}(K, -iD, t) \, dK \tag{38}$$

Writing $\tilde{z}(K, t) = a(K, -iD, t)$ we have

$$\frac{\partial \tilde{z}}{\partial t} = -(D + iK\sin\beta)\tilde{z} + (K/2)\left[\overline{R}e^{i\beta} - Re^{-i\beta}\tilde{z}^2\right] \tag{39}$$

where

$$R(t) = \int_0^\infty \Gamma(K)\overline{\tilde{z}}(K, t) \, dK \tag{40}$$

Moving to a rotating coordinate frame: $z \equiv \tilde{z}e^{i\Omega t}$ we see that z satisfies

$$\frac{\partial z}{\partial t} = -(D + i[K\sin\beta - \Omega])z + (K/2)\left[\overline{\widehat{R}}e^{i\beta} - \widehat{R}e^{-i\beta}z^2\right] \tag{41}$$

where

$$\widehat{R}(t) = \int_0^\infty \Gamma(K)\overline{z}(K,t)\, dK \tag{42}$$

Let us now compare our results with those of Ko and Ermentrout [13], derived using the self-consistency arguments of Kuramoto [14,7]. Ko and Ermentrout used identical oscillators, so set $D = 0$. Then, dropping the hat on $\widehat{R}$, steady states of (41) satisfy

$$KRe^{-i\beta}z^2 + 2i[K\sin\beta - \Omega]z - K\overline{R}e^{i\beta} = 0 \tag{43}$$

Solving for z and taking the positive square root we obtain

$$z = \frac{-i[K\sin\beta - \Omega] + \sqrt{K^2|R|^2 - (K\sin\beta - \Omega)^2}}{KRe^{-i\beta}} \tag{44}$$

At stationarity the phase of R is arbitrary so we can assume that R is real. Using (42) we obtain

$$R^2 = e^{-i\beta}\int_0^\infty \Gamma(K)\left(\frac{i[K\sin\beta - \Omega] + \sqrt{K^2R^2 - (K\sin\beta - \Omega)^2}}{K}\right) dK \tag{45}$$

which, after writing $\Delta = -\Omega$, is eqn. (17) in [13]. We note that $z = 0$ is always a solution of (41)-(42).

3.2 Results

Fig. 12 (top) shows a typical stationary solution of (41)-(42). Although these equations are solved on an evenly-spaced grid between K_{min} and K_{max} we plot the variables as a function of χ, where

$$\chi = h(K) \equiv \int_{K_{min}}^{K} \Gamma(s)\, ds \tag{46}$$

Because $0 < \Gamma(K)$, h is a monotonically increasing function with $h(K_{min}) = 0$ and $h(K_{max}) = 1$. Essentially, χ is the continuous analogue of index in (27), once the oscillators have been sorted by their K_i values, enabling easy comparison with results such as those in Fig. 11. The bottom panel of Fig. 12 shows, using colour, $\log[\widetilde{F}(\chi,\phi)]$, where

$$\widetilde{F}(\chi,\phi) \equiv \frac{1 - r^2(\chi)}{2\pi[1 - 2r(\chi)\cos(\phi - \theta(\chi)) + r^2(\chi)]} \tag{47}$$

Although the comparison with Fig. 11 is not exact, due to the non-zero value of D, the main features are the same.

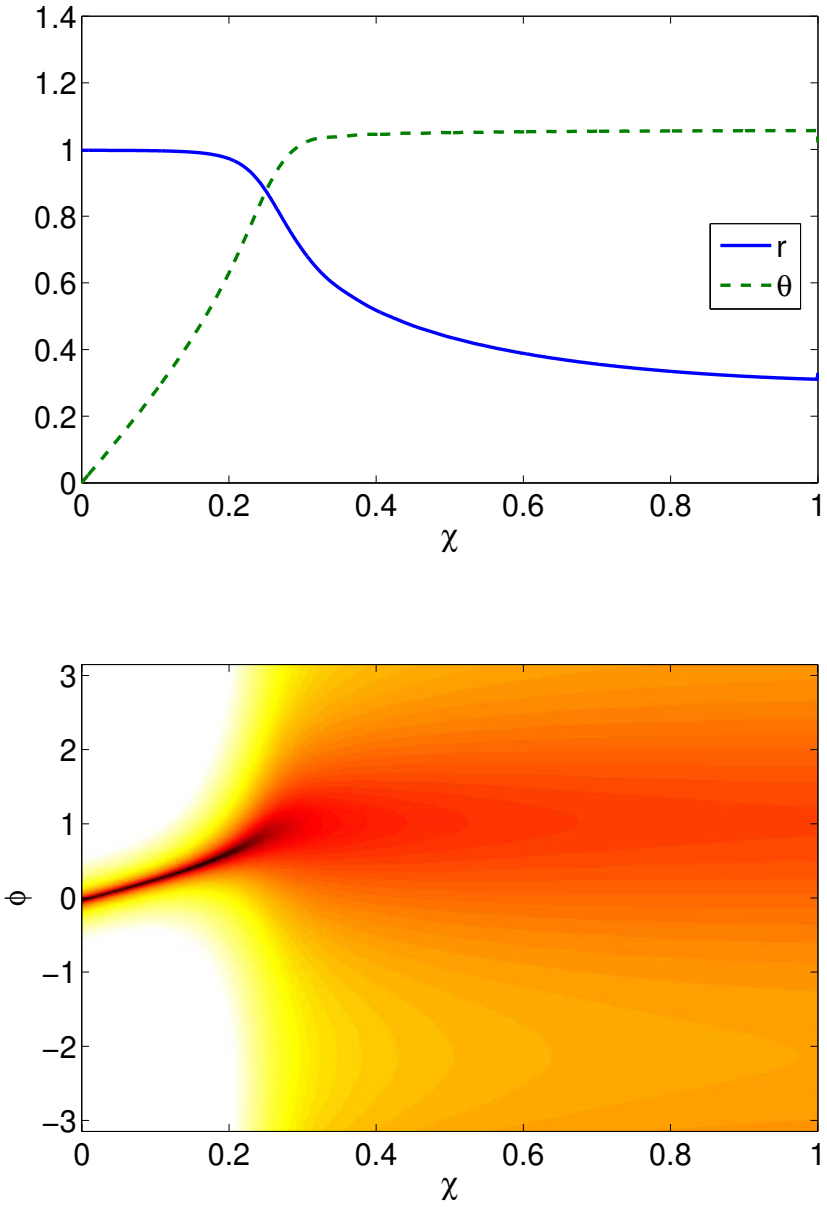

Fig. 12. Top: A stable stationary solution of (41)-(42) with $\Omega = 0.069031$ ($z = re^{-i\theta}$). We have set $\theta(0) = 0$. Bottom: $\log[\widetilde{F}(\chi,\phi)]$ (47) indicated with a colour code (black high, white low). Other parameters: $K_{min} = 0.1, K_{max} = 5, \gamma = 1.5, \beta = 0.4\pi, D = 0.0001$.

Figure 13 shows the result of continuing solutions of (41)-(42) as β is varied, for two different values of D, with stability indicated. The upper (lower) stable curves in the upper (lower) panel correspond to the solutions found by [13], while the other stable branches with $|R| \approx 1$ correspond to the in phase synchronous states found by them. (Note that these authors used identical oscillators, i.e. $D = 0$). The branches terminate for large β at pitchfork bifurcations involving the $z = 0$ (i.e. completely incoherent) state that is always a solution. This state is stable for β larger than the values at which

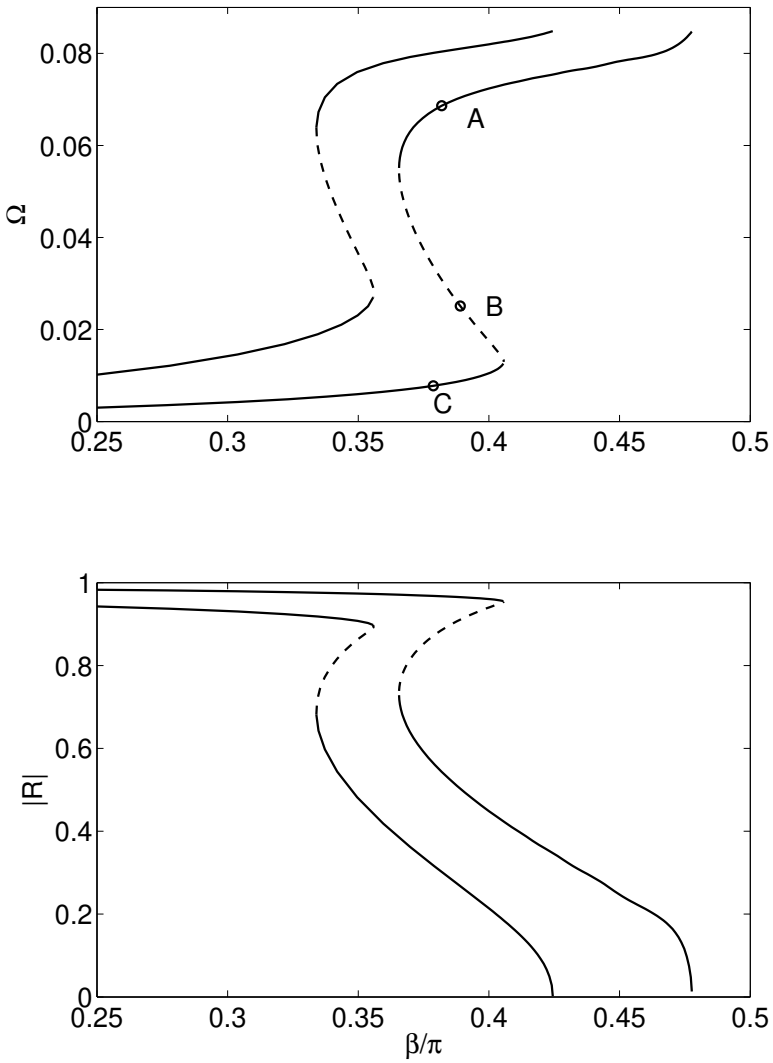

Fig. 13. Curves of stationary solutions of (41)-(42) for $D = 0.01$ (leftmost curves) and $D = 0.003$ (rightmost curves). Top: Ω and bottom: $|R|$ as a function of β. Solid line: stable, dashed line: unstable. Solutions at the points marked are shown in Fig. 14.

the curves in Fig. 13 terminate. This bifurcation diagram has been verified by simulating the original network (27) (not shown). Figure 14 shows $r(\chi)$ and $\theta(\chi)$ at the three points indicated in Fig. 13.

All of the results in this section are new, although Ko and Ermentrout [13] derived (45) using the self-consistency argument of Kuramoto and Battogtokh [14].

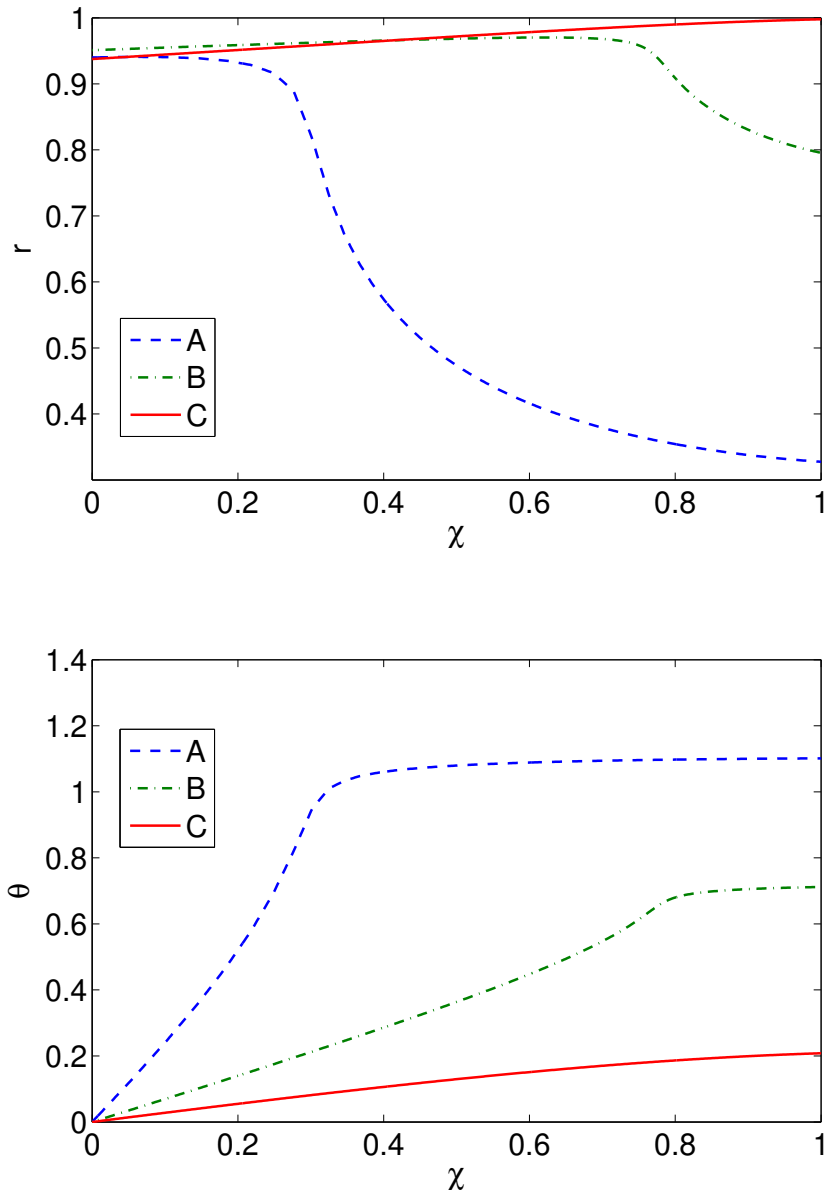

Fig. 14. Top: $r(\chi)$ and bottom: $\theta(\chi)$ at the three points indicated in Fig. 13. We have set $\theta(0) = 0$.

4 Spiral waves on a 2D lattice

We now consider spiral waves, a generic pattern in two-dimensional active media [24–26]. Shima and Kuramoto [15] considered the following system:

$$\frac{\partial \phi}{\partial t} = \omega - K \int G(|\mathbf{x} - \mathbf{y}|) \sin [\phi(\mathbf{x}) - \phi(\mathbf{y}) + \alpha] d\mathbf{y} \tag{48}$$

in $\mathbb{R}^2$ where

$$G(r) = \frac{1}{2\pi} K_0(r) \tag{49}$$

and K_0 is the modified Bessel function of the second kind. They found spiral waves with "phase-randomised cores," and showed their existence using the self-consistency argument of Kuramoto [14]. Kim et al. [27] also found spiral waves with phase-randomised cores in two-dimensional arrays of coupled phase oscillators, and it is their system that we study here. The equations are

$$\frac{d\phi_{ij}}{dt} = \omega_{ij} + \frac{1}{N_{ij}(\eta)} \sum_{mn}^{\sim} \sin\left(\phi_{mn} - \phi_{ij} - \alpha\right) \tag{50}$$

for $1 \leq i \leq N, 1 \leq j \leq N$, where (i, j) indicates the position on the lattice and $\sum_{mn}^{\sim}$ indicates a sum over all lattice points within a distance η of the point (i, j); there are $N_{ij}(\eta)$ of these. Note that we do not use periodic boundary conditions, so $N_{ij}(\eta)$ will be smaller for points near the boundary than for points well away from the boundary. A snapshot of a typical spiral for $\eta = 7$ is shown in Fig. 15. The unsynchronised oscillators at the spiral core are clearly visible.

While spiral waves in systems with local interactions have been studied by a number of authors [24,25,28], their behaviour in systems with non-local interactions, as is the case here, is much less well-studied [29].

4.1 Analysis

We do not move to a spatial continuum, but as usual assume the existence of a probability density function $f_{ij}(\omega, \phi, t)$ which satisfies the usual continuity equation (2), where

$$v = \omega_{ij} + \frac{1}{N_{ij}(\eta)} \sum_{mn}^{\sim} \int_{-\infty}^{\infty} \int_{-\pi}^{\pi} \sin\left(\phi_{mn} - \phi_{ij} - \alpha\right) f_{mn}(\omega, \phi_{mn}, t)\, d\phi_{mn}\, d\omega \tag{51}$$

Defining the order parameter

$$R_{ij} = \frac{1}{N_{ij}(\eta)} \sum_{mn}^{\sim} \int_{-\infty}^{\infty} \int_{-\pi}^{\pi} e^{i\phi_{mn}} f_{mn}(\omega, \phi_{mn}, t)\, d\phi_{mn}\, d\omega \tag{52}$$

we see that

$$v = \omega_{ij} + \frac{1}{2i}\left[R_{ij} e^{-i(\phi_{ij}+\alpha)} - \overline{R}_{ij} e^{i(\phi_{ij}+\alpha)}\right] \tag{53}$$

Writing

$$f_{ij}(\omega, \phi, t) = \frac{g(\omega)}{2\pi}\left[1 + \left\{\sum_{n=1}^{\infty} [a_{ij}(\omega, t)]^n e^{in\phi} + c.c.\right\}\right] \tag{54}$$

we find that

$$\frac{\mathrm{d}a_{ij}}{\mathrm{d}t} = -i\omega_{ij} a_{ij} + (1/2)\left[\overline{R}_{ij} e^{i\alpha} - R_{ij} e^{-i\alpha} a_{ij}^2\right] \tag{55}$$

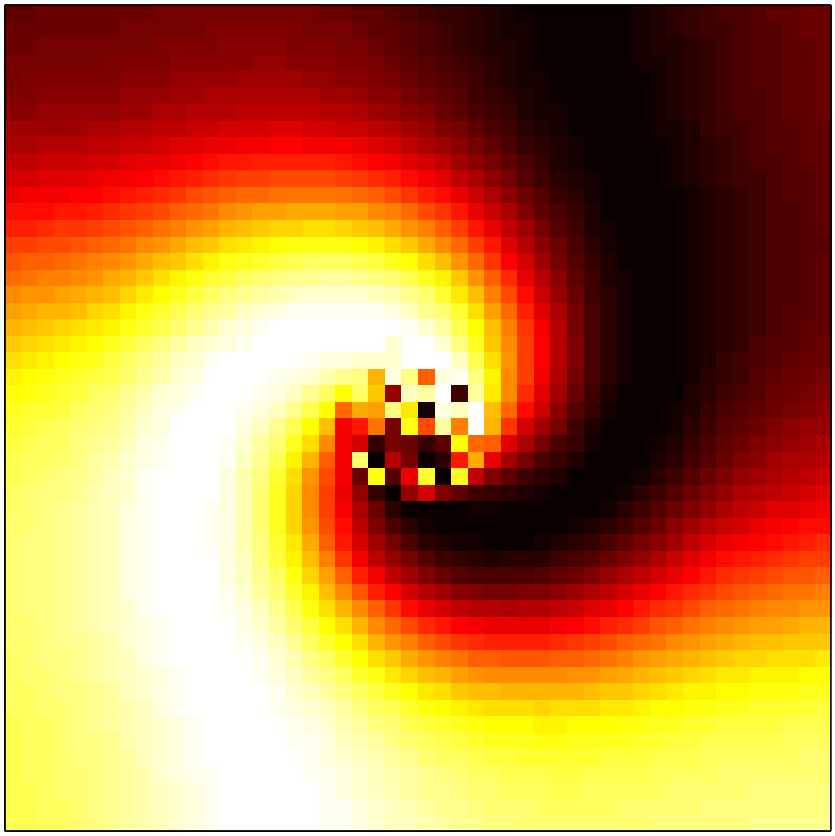

Fig. 15. Snapshot of a spiral wave ($\sin\phi_{ij}$ is shown colour-coded) for (50). $N = 50, \alpha = 0.2\pi, \eta = 7$ and $\omega_{ij} = 0.55\ \forall i, j$.

where

$$R_{ij} = \frac{1}{N_{ij}(\eta)} \sum_{mn}^{\sim} \int_{-\infty}^{\infty} g(\omega) \overline{a}_{mn}(\omega, t)\, d\omega \tag{56}$$

Using the usual $g(\omega)$ (37) we define $\tilde{z}_{ij}(t) = a_{ij}(-iD, t)$ so that

$$\frac{\mathrm{d}\tilde{z}_{ij}}{\mathrm{d}t} = -D\tilde{z}_{ij} + (1/2)\left[\overline{R}_{ij} e^{i\alpha} - R_{ij} e^{-i\alpha} \tilde{z}_{ij}^2\right] \tag{57}$$

where

$$R_{ij} = \frac{1}{N_{ij}(\eta)} \sum_{mn}^{\sim} \overline{\tilde{z}}_{mn}(t) \tag{58}$$

Writing $z_{ij} = \tilde{z}_{ij} e^{i\Omega t}$ we finally have

$$\frac{\mathrm{d}z_{ij}}{\mathrm{d}t} = -(D + i\Omega) z_{ij} + (1/2)\left[\overline{\widehat{R}}_{ij} e^{i\alpha} - \widehat{R}_{ij} e^{-i\alpha} z_{ij}^2\right] \tag{59}$$

where

$$\widehat{R}_{ij} = \frac{1}{N_{ij}(\eta)} \sum_{mn}^{\sim} \overline{z}_{mn}(t) \tag{60}$$

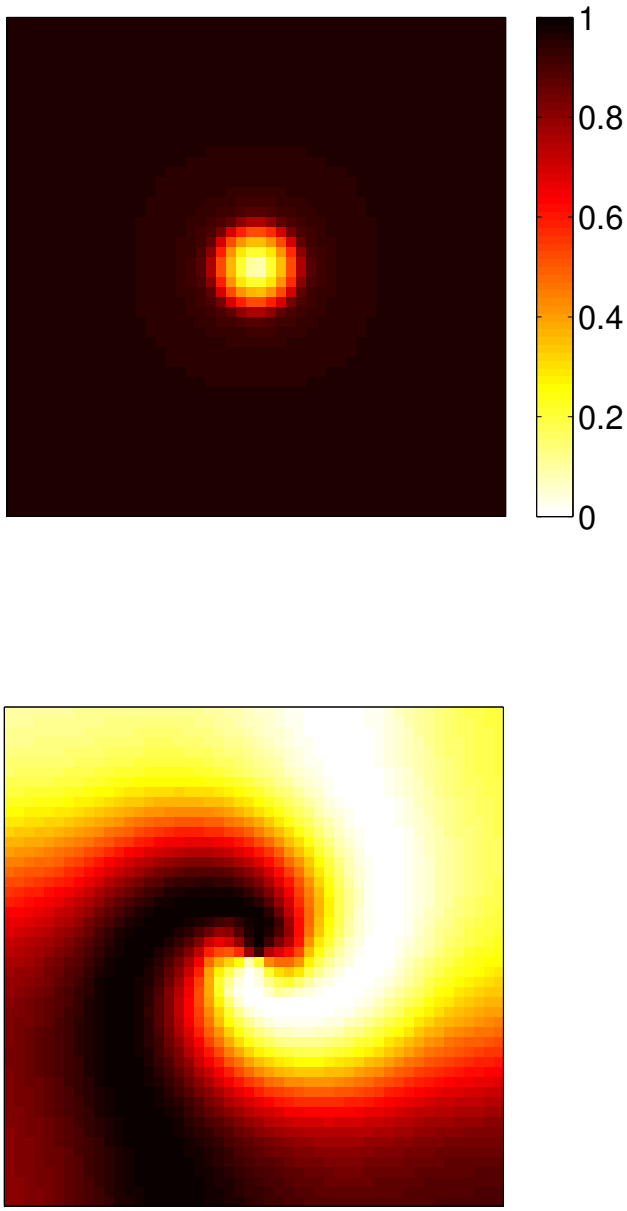

Fig. 16. Stable steady state of (59)-(60) with $\Omega = 0.50295$ and $D = 0.03$. Top: r_{ij}; bottom: $\sin\theta_{ij}$ (colour-coded), where $z_{ij} = r_{ij}e^{-i\theta_{ij}}$. $N = 50, \alpha = 0.2\pi, \eta = 7$.

4.2 Results

Figure 16 shows a stable steady state of (59)-(60) with $D = 0.03$. We see that for sites away from the centre of the domain, $|z_{ij}| \approx 1$, corresponding to highly synchronised oscillators, but there is a central core with $|z_{ij}|$ significantly less than 1, corresponding to the incoherent oscillators. Note that the phase of z_{ij} shows a typical spiral, with a phase singularity in the centre, in contrast to the spiral in the original network (Fig. 15).

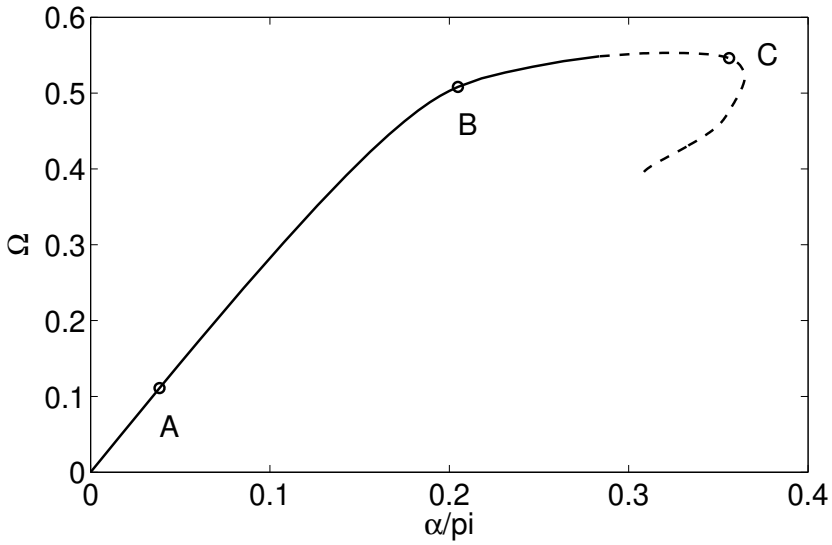

Fig. 17. Steady states of (59)-(60) with $D = 0.03$. Solid line: stable; dashed line: unstable. Solutions at the points marked are shown in Fig. 18.

4.2.1 Varying parameters

Varying α we obtain the family of spiral waves shown in Fig. 17. Several representative solutions are shown in Fig. 18. We see that as α is decreased, the width of the incoherent core decreases. (This was verified by simulations of (50), not shown.) Note that the square domain has a significant influence on the solution for large α, and further investigations of this system should probably use a circular domain [29,25].

4.2.2 Hopf bifurcation

We can also cause Hopf bifurcations in (59)-(60) by making α spatially-dependent, as in Sec. 2.2.2. We set $\alpha_{ij} = \alpha_0 + \alpha_1 \Phi_{ij}$, where

$$\Phi_{ij} = \exp\left(-5\left\{[(2i-51)/49]^2 + [(2j-51)/49]^2\right\}\right) \tag{61}$$

i.e. Φ_{ij} is a Gaussian, centred at the centre of the domain (recall that $N = 50$). In Fig. 19 we have plotted r along a horizontal slice through the centre of the domain, and show the effect of abruptly switching α_1 from 0 to 0.05π. The "spot" of low r simultaneously moves away from and starts to rotate about the centre of the domain, and the dynamics are analogous to those resulting from a Hopf bifurcation of a normal spiral wave [26,29]. Detecting and following the Hopf bifurcation, as in Sec. 2.2.2, should be possible, although time-consuming. The presence of this Hopf bifurcation was also verified in the original network (50) (not shown).

All of the results in the section, obtained using the OA ansatz, are new.

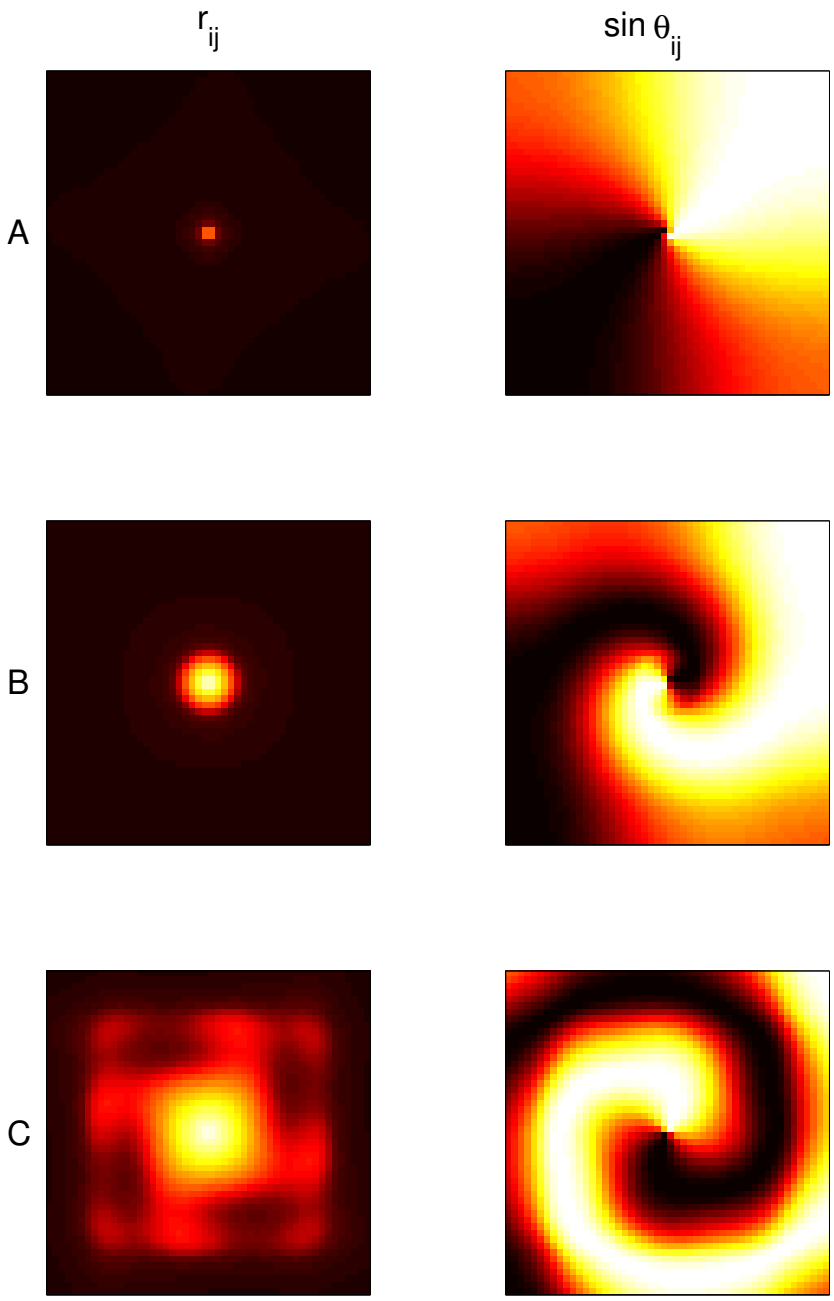

Fig. 18. Steady states of (59)-(60) at the three points indicated in Fig. 17. Left column: r_{ij} (black: high; white: low) ; right column: $\sin\theta_{ij}$.

5 Other models

We now consider several models which are similar to that studied in Sec. 2, although both include delays.

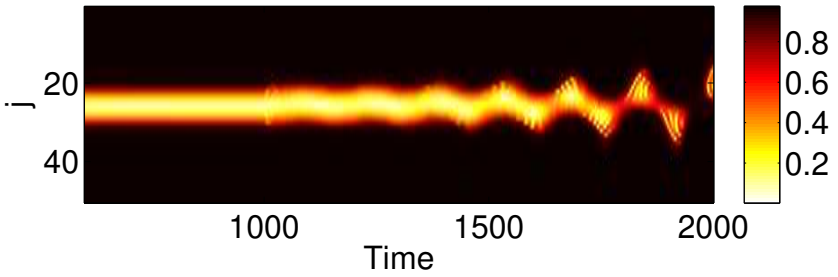

Fig. 19. r_{25j} when α_1 is switched from 0 to 0.05π at $t = 1000$. $D = 0.02, \alpha_0 = 0.2\pi$.

5.1 *Omel'chenko et al.*

Omel'chenko et al. [11] studied the model

$$\frac{\partial \phi}{\partial t} = \omega - \frac{C}{2}\int_{-1}^{1} \sin\left[\phi(x,t) - \phi(y,t)\right] dy - \frac{K\rho(x)}{2}\int_{-1}^{1} \sin\left[\phi(x,t) - \phi(y,t-\tau)\right] dy \tag{62}$$

where

$$\rho(x) = \frac{a e^{-a|x|}}{1 - e^{-a}} \tag{63}$$

and $0 < a$.

5.1.1 *Analysis*

Define a density function $f(x, \omega, \phi, t)$ which satisfies (2) where

$$\begin{aligned} v = \omega &- \frac{C}{2}\int_{-1}^{1}\int_{-\infty}^{\infty}\int_{-\pi}^{\pi} \sin\left[\phi(t) - \phi'(t)\right] f(y,\omega,\phi',t)\, d\phi'\, d\omega\, dy \\ &- \frac{K\rho(x)}{2}\int_{-1}^{1}\int_{-\infty}^{\infty}\int_{-\pi}^{\pi} \sin\left[\phi(t) - \phi'(t-\tau)\right]\, f(y,\omega,\phi',t)\, d\phi'\, d\omega\, dy \end{aligned} \tag{64}$$

where $\phi = \phi(x)$ and $\phi' = \phi(y)$. Defining the (spatially-independent) order parameter

$$R(t) = \frac{1}{2}\int_{-1}^{1}\int_{-\infty}^{\infty}\int_{-\pi}^{\pi} e^{i\phi'(t)} f(y,\omega,\phi',t) d\phi'\, d\omega\, dy \tag{65}$$

we can rewrite

$$v = \omega - \frac{C}{2i}\left[\overline{R}(t)e^{i\phi} - R(t)e^{-i\phi}\right] - \frac{K\rho(x)}{2i}\left[\overline{R}(t-\tau)e^{i\phi} - R(t-\tau)e^{-i\phi}\right] \tag{66}$$

Writing

$$f(x,\omega,\phi,t) = \frac{g(\omega)}{2\pi}\left[1 + \left\{\sum_{n=1}^{\infty}[a(x,\omega,t)]^n e^{in\phi} + c.c.\right\}\right] \tag{67}$$

we find that a satisfies

$$\frac{\partial a}{\partial t} = -i\omega a + \frac{1}{2}\left[C\overline{R}(t) + K\rho(x)\overline{R}(t-\tau) - a^2\left\{CR(t) + K\rho(x)R(t-\tau)\right\}\right] \tag{68}$$

where

$$R(t) = \frac{1}{2}\int_{-1}^{1}\int_{-\infty}^{\infty} g(\omega)\bar{a}(y,\omega,t)\, d\omega\, dy \tag{69}$$

Because we are considering a delay system we can no longer assume without loss of generality that the mean of $g(\omega)$ is zero. We use $g(\omega)$ given by (9), and defining $\tilde{z}(x,t) = a(x,\omega_0 - iD,t)$ we obtain

$$\frac{\partial \tilde{z}}{\partial t} = -(i\omega_0 + D)\tilde{z} + \frac{1}{2}\left[C\overline{R}(t) + K\rho(x)\overline{R}(t-\tau) - \tilde{z}^2\left\{CR(t) + K\rho(x)R(t-\tau)\right\}\right] \tag{70}$$

where

$$R(t) = \frac{1}{2}\int_{-1}^{1} \bar{\tilde{z}}(t)\, dy \tag{71}$$

and letting $z = \tilde{z}e^{i\Omega t}$ we obtain

$$\begin{aligned}\frac{\partial z}{\partial t} &= -(D + i[\omega_0 - \Omega])z \\ &\quad + \frac{1}{2}\left[C\overline{\widehat{R}}(t) + K\rho(x)\overline{\widehat{R}}(t-\tau)e^{i\Omega\tau}\right. \\ &\quad \left. - z^2\left\{C\widehat{R}(t) + K\rho(x)\widehat{R}(t-\tau)e^{-i\Omega\tau}\right\}\right]\end{aligned} \tag{72}$$

where

$$\widehat{R}(t) = \frac{1}{2}\int_{-1}^{1} \bar{z}(t)\, dy \tag{73}$$

5.1.2 Results

Fig. 20 shows snapshots of solutions of the spatially-discretised version of (62) for two different values of τ, found using the Matlab routine `dde23`. Other parameters, as used by [11], are $a = 1, C = 0.1\pi, K = \pi, \omega = \omega_0 = 2\pi$. In Fig. 21 we show stable stationary solutions of (72)-(73) for the same parameter values as in Fig. 20, for $D = 0$. We see excellent agreement between the results for a finite network and those from the analysis of the corresponding PDE.

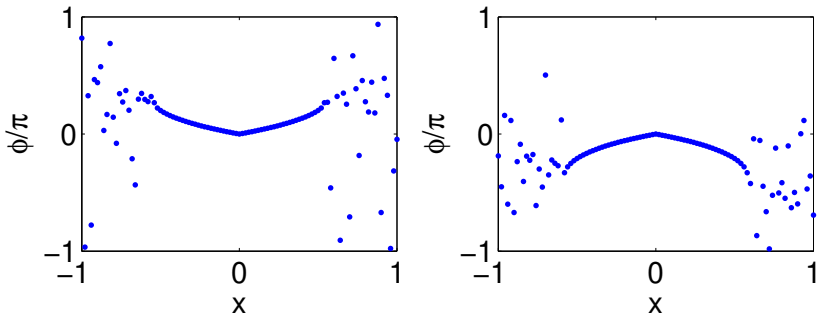

Fig. 20. Snapshots of solutions of the spatially-discretised version of (62) for $\tau = 0.3$ (left) and $\tau = 0.6$ (right). Compare with Fig. 1 in[11]. 101 oscillators are used. See text for other parameters.

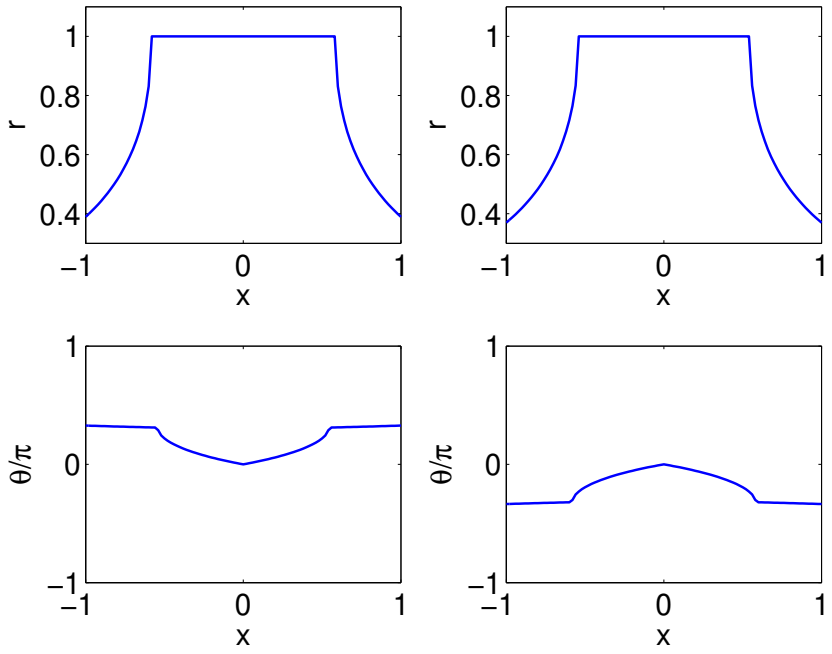

Fig. 21. Stable stationary solutions of (72)-(73) for $\tau = 0.3, \Omega = 4.0565$ (left) and $\tau = 0.6, \Omega = 8.4981$ (right) and $D = 0$. Same parameters as in Fig. 20. We have set $\theta(0) = 0$ to match the results in Fig. 20.

5.2 Sethia et al.

Sethia et al. [9] studied the model

$$\frac{\partial \phi}{\partial t} = \omega - \int_{-L}^{L} G(x-y) \sin\left[\phi(x,t) - \phi(y, t - |x-y|/V) + \alpha\right] dy \qquad (74)$$

on a ring of circumference $2L$, where

$$G(x) = \frac{k e^{-k|x|}}{2(1 - e^{-kL})} \qquad (75)$$

and V can be thought of as the speed of propagation of signals around the ring.

5.2.1 Analysis

Defining a density function $f(x, \omega, \phi, t)$ results in the usual continuity equation (2) where

$$v = \omega - \int_{-L}^{L} G(x-y) \int_{-\infty}^{\infty} \int_{-\pi}^{\pi} \sin\left[\phi(t) - \phi'(t - |x-y|/V) + \alpha\right] f(y, \omega, \phi', t) d\phi' d\omega dy$$

where $\phi = \phi(x)$ and $\phi' = \phi(y)$. Defining the order parameter

$$R(x,t) \equiv \int_{-L}^{L} G(x-y) \int_{-\infty}^{\infty} \int_{-\pi}^{\pi} e^{i\phi'(t-|x-y|/V)} f(y, \omega, \phi', t) d\phi' \, d\omega \, dy \tag{76}$$

we have

$$v(\phi, t) = \omega - \frac{1}{2i}\left[\overline{R} e^{i(\phi+\alpha)} - R e^{-i(\phi+\alpha)}\right]$$

Writing

$$f(x, \omega, \phi, t) = \frac{g(\omega)}{2\pi}\left[1 + \left\{\sum_{n=1}^{\infty} [a(x, \omega, t)]^n e^{in\phi} + c.c.\right\}\right] \tag{77}$$

we find

$$\frac{\partial a}{\partial t} = -i\omega a + \frac{1}{2}\left[\overline{R} e^{i\alpha} - R e^{-i\alpha} a^2\right] \tag{78}$$

where

$$R(x,t) = \int_{-L}^{L} G(x-y) \int_{-\infty}^{\infty} g(\omega) \overline{a}(y, \omega, t - |x-y|/V) \, d\omega \, dy \tag{79}$$

Using $g(\omega)$ from (9) and defining $\tilde{z}(x,t) = a(x, \omega_0 - iD, t)$ we obtain

$$\frac{\partial \tilde{z}}{\partial t} = -(i\omega_0 + D)\tilde{z} + \frac{1}{2}\left[\overline{R} e^{i\alpha} - R e^{-i\alpha} \tilde{z}^2\right] \tag{80}$$

where

$$R(x,t) = \int_{-L}^{L} G(x-y) \overline{\tilde{z}}(y, t - |x-y|/V) \, dy \tag{81}$$

and letting $z = \tilde{z} e^{i\Omega t}$ we have

$$\frac{\partial z}{\partial t} = -(D + i[\omega_0 - \Omega])z + \frac{1}{2}\left[\overline{\widehat{R}} e^{i\alpha} - \widehat{R} e^{-i\alpha} z^2\right] \tag{82}$$

where

$$\widehat{R}(x,t) = \int_{-L}^{L} G(x-y) \overline{z}(y, t - |x-y|/V) e^{-i\Omega|x-y|/V} \, dy \tag{83}$$

In the usual way, steady states of (82) when $D = 0$ are the same as those found using the self-consistency argument, see eqn. (6) in [9].

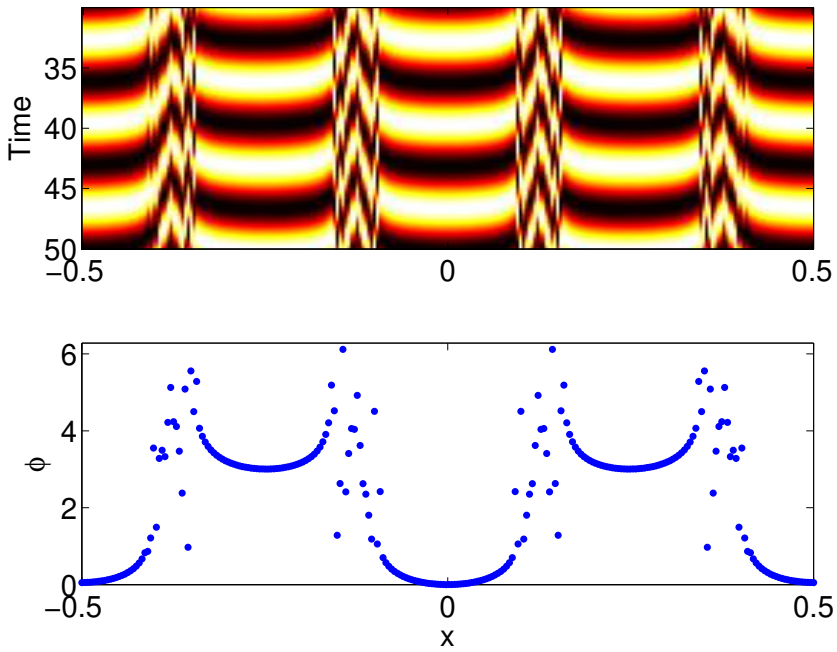

Fig. 22. A solution of the spatially-discretised version of (74). Top: $\sin\phi$ (colour-coded) over a time interval of length 20. Bottom: a snapshot of the ϕ. We have discretised with 256 spatial points and other parameters are $\omega = 1.1, \alpha = 0.9, V = 1/10.24, k = 4, L = 1/2$.

5.2.2 Results

In Fig. 22 we show a typical solution of the spatially-discretised version of (74), using the same parameters as [9]. We see four coherent regions (the domain is periodic in x), adjacent ones of which are out of phase, separated by regions of incoherence.

In Fig. 23 we show a stationary solution of (82)-(83) for $D = 0$ and the same other parameters as in Fig. 22. The correspondence with Fig. 22 is excellent. As noted by [9], the solution shown in Fig. 23 is only stable in the space of spatially-even functions. If this symmetry is not preserved, (82)-(83) have stable travelling wave solutions, for which r is constant and θ is a linearly increasing function of space and time (not shown).

6 Discussion

In this paper we have considered a number of infinite networks of coupled heterogeneous phase oscillators. For each network we used the OA ansatz [16] to derive a PDE, the solutions of which describe the dynamics of the network. Of course, for each network a more general such PDE exists: the continuity equation (2). However, the power of the OA ansatz is that it

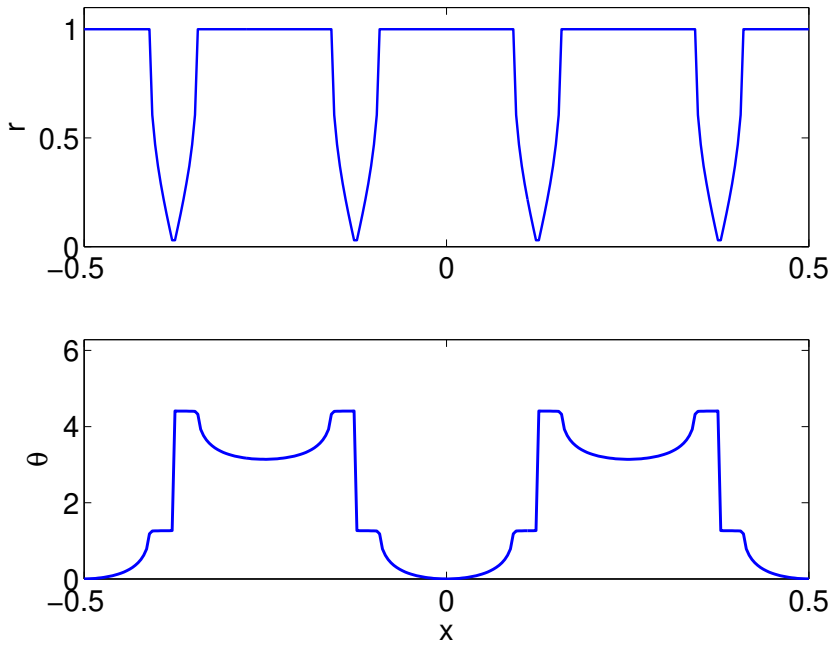

Fig. 23. A stationary solution of (82)-(83) for $D = 0$ and $\Omega = 0.90869$. Top: $r(x)$; bottom: $\theta(x)$ ($z = re^{-i\theta}$). Other parameters are $\omega = 1.1, \alpha = 0.9, V = 1/10.24, k = 4, L = 1/2$.

reduces by one the number of variables in the PDE that needs to be studied. For example, for the model considered in Sec 2, eqn. (2) is a PDE for f, which is a function of four variables, x, ω, ϕ and t. The OA ansatz removes the dependence on ϕ and we obtain the PDE (7) for a function of only three variables. The dependence on ω can be integrated out by choosing $g(\omega)$ to be, for example, a Lorentzian or Dirac delta function, and we obtain (13), a PDE for $z(x,t)$. Similarly in Sec. 3 we obtain the PDE (41) for the variable z, which is a function of only K (a space-like variable) and t, and in Sec. 4 we obtain the spatially-indexed ODEs (59).

Effectively, we have greatly generalised the results of Marvel and Strogatz [30], who showed that any system of N identical oscillators governed by the dynamics

$$\frac{\mathrm{d}\phi_j}{\mathrm{d}t} = \mu e^{-i\phi_j} + \lambda + \overline{\mu} e^{i\phi_j} \tag{84}$$

could be solved using the OA ansatz: assume a density

$$\rho(\phi, t) = \frac{1}{2\pi}\left[1 + \sum_{n=1}^{\infty}\left\{\alpha(t)e^{i\phi}\right\}^n + c.c\right] \tag{85}$$

Then α satisfies the ODE

$$\frac{\mathrm{d}\alpha}{\mathrm{d}t} = -i(\lambda\alpha + \overline{\mu} + \mu\alpha^2) \tag{86}$$

Marvel and Strogatz stated that the OA ansatz requires identical oscillators

and that f and g be independent of the oscillator index. In fact, we have shown here that we can relax both of these assumptions and still use the OA ansatz, but the price we pay is that we now have a PDE (or N ODEs). For example, in Sec. 2 we find the velocity of each oscillator is given by (5):

$$v = \omega - \left[Re^{i(\phi-\beta)} + \bar{R}e^{-i(\phi-\beta)}\right]/2 \tag{87}$$

which is of the form (84), with $\lambda = \omega$ and $\mu = -\overline{R}e^{i\beta}/2$. Here, R is a function of space (or oscillator index, in the discrete case) and we obtain the PDE (7)

$$\frac{\partial a}{\partial t} = -i\omega a + (i/2)\left[Re^{-i\beta} + \bar{R}e^{i\beta}a^2\right] \tag{88}$$

where a is now a function of space too. Similarly, in Sec. 3 we obtain (33)

$$v = \omega + K\sin\beta + \frac{K}{2i}\left[Re^{-i(\phi+\beta)} - \overline{R}e^{i(\phi+\beta)}\right] \tag{89}$$

where R is the same for each oscillator. However, K is different for each oscillator (or K is a continuous variable, in the continuum limit) so we obtain the PDE (35):

$$\frac{\partial a}{\partial t} = -i(\omega + K\sin\beta)a + (K/2)[\overline{R}e^{i\beta} - Re^{-i\beta}a^2] \tag{90}$$

where a is a function of K as well as t.

We have only considered solutions of the PDEs derived in this paper when D (the width of the distribution from which intrinsic frequencies are drawn) is not zero (though see Figs. 21 and 23 for exceptions). The correctness of using the OA ansatz to describe stable states of the networks studied here has been the subject of recent discussion [17,30,19,31]. For example, Pikovsky and Rosenblum [17] recently demonstrated using the Watanabe-Strogatz (WS) ansatz [18] that the OA ansatz did not completely describe all of the dynamics possible in the network studied by Abrams et al. [8]. However, there is mounting numerical evidence that the OA ansatz does in fact describe all attracting (and, presumably, hyperbolic) states, if the oscillators in the network are non-identical [12,31,16,17,19]. The recent preprint by Ott and Antonsen [32] seems to put these observations on a sound theoretical basis. To correctly study the networks considered in this paper when the oscillators are identical it may be necessary to generalise the WS ansatz to these topologies [33], or it may be that the dynamics really are described by equations such as (13), (41), (59), (72) and (82) with $D = 0$. We leave the connection between the WS and OA ansätze, and the analysis of the equations just mentioned when $D = 0$ for future work.

Regarding the dependence of the results on the specific form of $g(\omega)$: other distributions with similar pole structures in the complex plane could be

used, resulting in similar (although more complicated) equations [12,16]. Numerical results with other distributions (e.g. Gaussian) suggest that there is nothing special about the Lorentzian distribution [12,19,31].

In summary, our main result is the demonstration that a number of different networks, each capable of supporting "chimera" (and other) states, can be analysed using the same framework. We have discovered new types of behaviour, and put on a solid footing the stability results inferred by others [13,11,7,10,12]. The results presented here are by no means complete; further analysis of the PDEs derived should result in the discovery of more interesting behaviour of coupled oscillator networks.

Acknowledgements

I thank the referees for their useful comments, and for bringing the preprint [32] to my attention.

References

[1] S. Strogatz. *Sync: The Emerging Science of Spontaneous Order*. Hyperion, 2003.

[2] A. Pikovsky, M. Rosenblum, and J. Kurths. *Synchronization*. Cambridge University Press, 2001.

[3] A.T. Winfree. *The Geometry of Biological Time*. Springer, 2001.

[4] J.A. Acebrón, LL Bonilla, C.J. Pérez Vicente, F. Ritort, and R. Spigler. The Kuramoto model: A simple paradigm for synchronization phenomena. *Rev. Mod. Phys.*, 77:137–185, 2005.

[5] Yoshiki. Kuramoto. *Chemical oscillations, waves, and turbulence*. Springer-Verlag, 1984.

[6] S.H. Strogatz. From Kuramoto to Crawford: exploring the onset of synchronization in populations of coupled oscillators. *Physica D*, 143:1–20, 2000.

[7] Daniel M. Abrams and Steven H. Strogatz. Chimera states in a ring of nonlocally coupled oscillators. *Int. J. Bifn. Chaos*, 16:21–37, 2006.

[8] Daniel M. Abrams, Rennie Mirollo, Steven H. Strogatz, and Daniel A. Wiley. Solvable model for chimera states of coupled oscillators. *Phys. Rev. Lett.*, 101:084103, 2008.

[9] G.C. Sethia, A. Sen, and F.M. Atay. Clustered Chimera States in Delay-Coupled Oscillator Systems. *Phys. Rev. Lett.*, 100:144102, 2008.

[10] Daniel M. Abrams and Steven H. Strogatz. Chimera states for coupled oscillators. *Phys. Rev. Lett.*, 93:174102, 2004.

[11] O.E. Omel'chenko, Y.L. Maistrenko, and P.A. Tass. Chimera States: The Natural Link Between Coherence and Incoherence. *Phys. Rev. Lett.*, 100:044105, 2008.

[12] Carlo R. Laing. Chimera states in heterogeneous networks. *Chaos*, 19:013113, 2009.

[13] T.W. Ko and G.B. Ermentrout. Partially locked states in coupled oscillators due to inhomogeneous coupling. *Physical Review E*, 78(1):016203, 2008.

[14] Y. Kuramoto and D. Battogtokh. Coexistence of Coherence and Incoherence in Nonlocally Coupled Phase Oscillators. *Nonlinear Phenom. Complex Syst.*, 5:380–385, 2002.

[15] S. Shima and Y. Kuramoto. Rotating spiral waves with phase-randomized core in nonlocally coupled oscillators. *Physical Review E*, 69(3):036213, 2004.

[16] Edward Ott and Thomas M. Antonsen. Low dimensional behavior of large systems of globally coupled oscillators. *Chaos*, 18:037113, 2008.

[17] Arkady Pikovsky and Michael Rosenblum. Partially integrable dynamics of hierarchical populations of coupled oscillators. *Phys. Rev. Lett.*, 101:264103, 2008.

[18] S. Watanabe and SH Strogatz. Constants of motion for superconducting Josephson arrays. *Physica. D*, 74:197–253, 1994.

[19] E. A. Martens, E. Barreto, S. H. Strogatz, E. Ott, P. So, and T. M. Antonsen. Exact results for the kuramoto model with a bimodal frequency distribution. *Physical Review E*, 79:026204, 2009.

[20] J. Guckenheimer and P. Holmes. *Nonlinear Oscillations, Dynamical Systems, and Bifurcations of Vector Fields*. Springer, 1983.

[21] Y.A. Kuznetsov. *Elements of Applied Bifurcation Theory*. Springer, 2004.

[22] E. Doedel, RC Paffenroth, AR Champneys, TF Fairgrieve, Y.A. Kuznetsov, B. Sandstede, and X. Wang. AUTO 2000: Continuation and Bifurcation Software for Ordinary Differential Equations (with HomCont). *Concordia University, Canada, ftp. cs. concordia. ca/pub/doedel/auto*.

[23] C. Laing and S. Coombes. The importance of different timings of excitatory and inhibitory pathways in neural field models. *Network: Computation in Neural Systems*, 17(2):151–172, 2006.

[24] M. Bär, A.K. Bangia, and I.G. Kevrekidis. Bifurcation and stability analysis of rotating chemical spirals in circular domains: Boundary-induced meandering and stabilization. *Physical Review E*, 67(5):056126, 2003.

[25] D. Barkley. Linear stability analysis of rotating spiral waves in excitable media. *Physical Review Letters*, 68(13):2090–2093, 1992.

[26] D. Barkley. Euclidean symmetry and the dynamics of rotating spiral waves. *Physical Review Letters*, 72(1):164–167, 1994.

[27] P.J. Kim, T.W. Ko, H. Jeong, and H.T. Moon. Pattern formation in a two-dimensional array of oscillators with phase-shifted coupling. *Physical Review E*, 70(6):065201, 2004.

[28] G. Bordyugov and H. Engel. Continuation of spiral waves. *Physica D: Nonlinear Phenomena*, 228(1):49–58, 2007.

[29] C.R. Laing. Spiral waves in nonlocal equations. *SIAM Journal on Applied Dynamical Systems*, 4(3):588–606, 2005.

[30] Seth A. Marvel and Steven H. Strogatz. Invariant submanifold for series arrays of josephson junctions. *Chaos: An Interdisciplinary Journal of Nonlinear Science*, 19(1):013132, 2009.

[31] L.M. Childs and S.H. Strogatz. Stability diagram for the forced Kuramoto model. *Chaos: An Interdisciplinary Journal of Nonlinear Science*, 18:043128, 2008.

[32] Edward Ott and Thomas M. Antonsen. Long Time Evolution of Phase Oscillator Systems. *Arxiv preprint arXiv:0902.2773v1*, 2009.

[33] Seth A. Marvel, Renato E. Mirollo, and Steven H. Strogatz. Sinusoidally coupled phase oscillators evolve by Möbius group action. *Arxiv preprint*, arXiv:0904.1680v1, 2009.